RadioGraphics

Orbital Neoplasms in Adults: Clinical, Radiologic, and Pathologic Review[1]

Tina D. Tailor, MD • Divakar Gupta, MD • Roberta W. Dalley, MD
C. Dirk Keene, MD, PhD • Yoshimi Anzai, MD, MPH

ONLINE-ONLY SA-CME

See www.rsna.org/education/search/RG

LEARNING OBJECTIVES

After completing this journal-based SA-CME activity, participants will be able to:

- Describe the basic anatomy of the orbit.
- Recognize imaging features of orbital neoplasms and explain their histologic basis.
- Formulate a differential diagnosis for adult orbital neoplasms on the basis of their location and imaging features.

TEACHING POINTS

See last page

Orbital neoplasms in adults may be categorized on the basis of location and histologic type. Imaging features of these lesions often reflect their tissue composition. Cavernous malformations (also known as cavernous hemangiomas), although not true neoplasms, are the most common benign adult orbital tumor. They typically appear as a well-circumscribed, ovoid intraconal mass on cross-sectional images. Lymphoma, which may be primary or secondary to systemic disease, is the most prevalent orbital neoplasm in older adults (≥60 years of age). Choroidal melanoma is the most common primary adult ocular malignancy. Melanin has intrinsic T1 and T2 shortening effects, classically manifesting with hyperintense signal on T1-weighted magnetic resonance (MR) images and with hypointense signal on T2-weighted images. However, amelanotic or mildly pigmented lesions of melanoma do not demonstrate these characteristic MR imaging features. Breast cancer is the most common malignancy to metastasize to the orbit, followed by prostate cancer, melanoma, and lung cancer. In women with bilateral enophthalmos, metastatic scirrhous breast cancer should be considered in the differential diagnosis. Neoplasms that arise from the optic nerve or its sheath include glioma and meningioma. At imaging, gliomas often cause fusiform expansion of the optic nerve, in which the nerve itself cannot be delineated from the lesion. In contrast, meningiomas classically have a "tram-track" configuration, whereby the contrast-enhancing tumor is seen alongside the optic nerve. Neoplasms that derive from peripheral nerves include schwannoma and neurofibroma, the latter of which is associated with neurofibromatosis type 1. MR imaging is particularly valuable for evaluation of orbital neoplasms, as it provides critical anatomic information about ocular structures involved, perineural spread, and intracranial extension.

Introduction

Orbital neoplasms in adults comprise a broad spectrum of benign and malignant entities. Cross-sectional imaging plays a valuable role in characterization of these lesions and in evaluation of disease extent, supplementing clinical ophthalmologic examination and providing information beyond what can be seen at fundoscopy. As with imaging evaluation of all orbital disease processes, a general approach

Abbreviations: ADC = apparent diffusion coefficient, NF-1 = neurofibromatosis type 1

RadioGraphics 2013; 33:1739–1758 • **Published online** 10.1148/rg.336135502 • **Content Codes:** HN MR NR OI

[1]From the Departments of Radiology (T.D.T., R.W.D., Y.A.), Ophthalmology (D.G., C.D.K.), and Pathology (C.D.K.), University of Washington Medical Center, 1959 NE Pacific St, Box 357115, Seattle, WA 98195-7115. Recipient of a Certificate of Merit award for an education exhibit at the 2012 RSNA Annual Meeting. Received February 1, 2013; revision requested March 4 and received March 23; accepted April 3. For this journal-based SA-CME activity, the authors, editor, and reviewers have no financial relationships to disclose. **Address correspondence to** T.D.T. (e-mail: *tailort@uw.edu*).

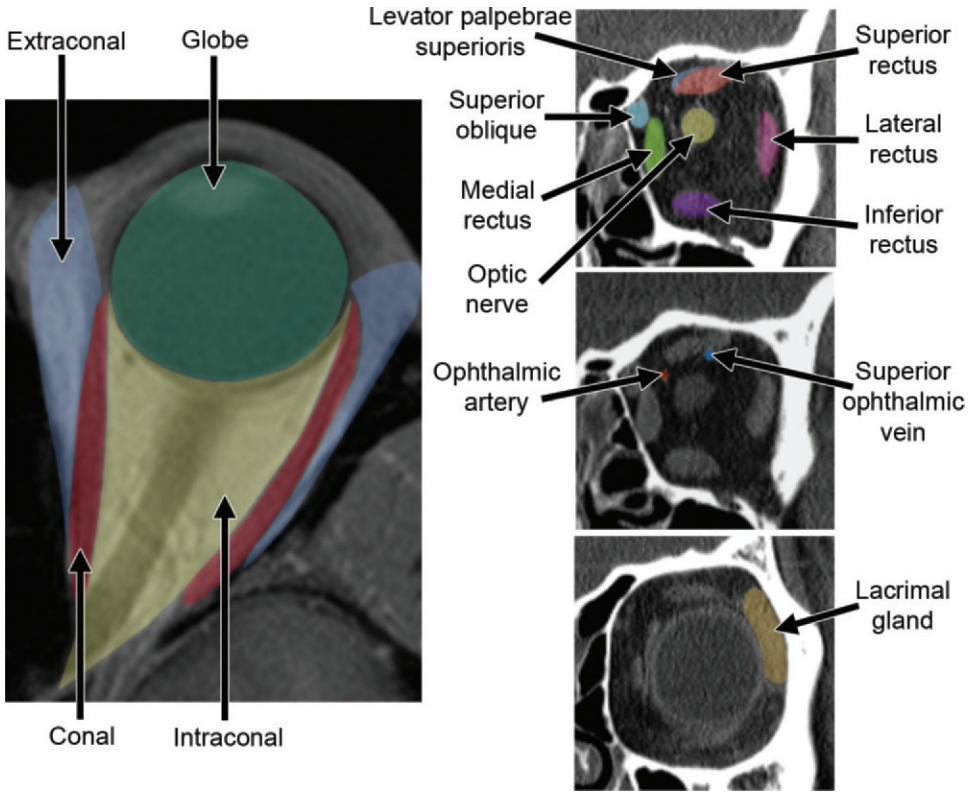

Figure 1. Normal orbital anatomy. Axial computed tomographic (CT) image (left) with color overlays shows the orbit divided into intraocular and extraocular spaces by the muscle cone and their relationships to the globe. Coronal CT images (right) with color overlays show the configuration of the extraocular muscles, vascular structures, and lacrimal gland.

should consider the anatomic compartment of involvement. In addition, in the evaluation of known or suspected neoplasm, consideration should also be given to the various tissues of origin from which neoplasms arise. In this regard, Shields et al conducted a large case study, evaluating 1264 consecutive patients referred to an ocular oncology service for suspected orbital tumor or tumor-simulating condition (1). In their series, vasculogenic lesions were the most common (17% of cases), followed by lymphoid, lacrimal gland, optic nerve and meningeal, metastatic, peripheral nerve, and primary melanoma lesions. Although melanoma was the most common primary ocular malignancy in their series, melanoma constituted 1% of all lesions evaluated. Other relatively rare lesions include fibrocytic, myogenic, lipogenic, and myxoid tumors.

In this article, the clinical, histopathologic, and imaging features of the more common nonosseous orbital neoplasms in the adult population are discussed.

Table 1
Contents of the Intraconal and Extraconal Compartments

Intraconal compartment
Fat
Cranial nerves: optic nerve, oculomotor nerve, nasociliary branch of the ophthalmic nerve, abducens nerve
Ciliary ganglion
Ophthalmic artery
Extraconal compartment
Fat
Cranial nerves: lacrimal and frontal branches of the ophthalmic nerve, trochlear nerve
Lacrimal gland

Anatomic Considerations

A basic understanding of orbital anatomy is critical in evaluation of orbital neoplasms. Not only can site of involvement guide the differential diagnostic considerations, but accurate descriptions of lesion location, involved structures, and extent of dissemination can facilitate proper treatment planning.

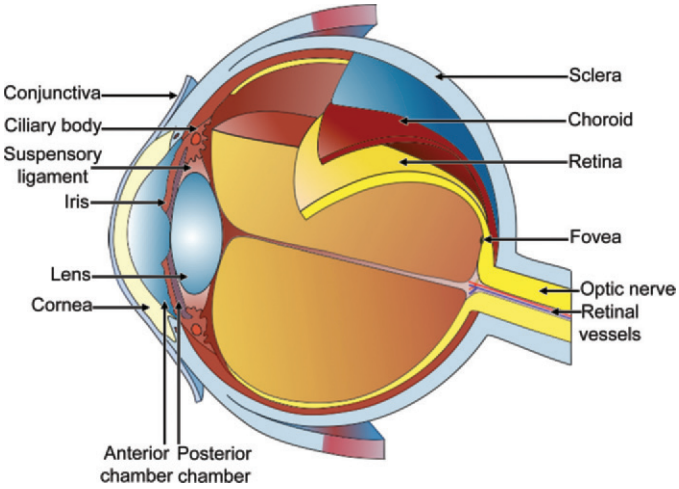

Figure 2. Diagram illustrates the cross-sectional anatomy of the globe.

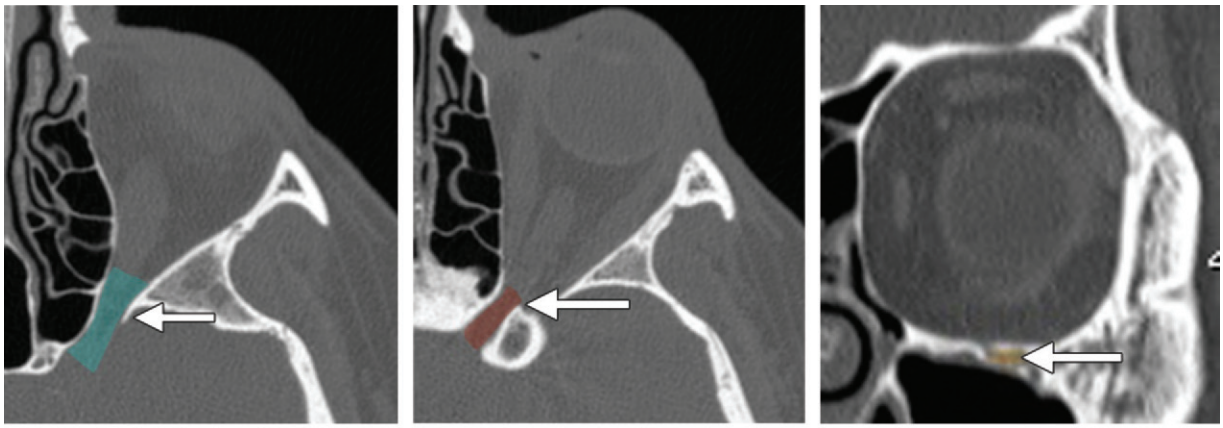

Figure 3. Orbital foramina. Axial **(a, b)** and coronal **(c)** CT bone-window images demonstrate the superior orbital fissure (arrow, blue overlay in **a**), optic canal (arrow, brown overlay in **b**), and infraorbital canal (arrow, yellow overlay in **c**). Contents of each foramen are shown in Table 2.

The orbit is divided into the ocular compartment or globe, the muscle cone, and intraconal and extraconal spaces (Fig 1). Six extraocular muscles control ocular movements; all but the inferior oblique muscle constitute the muscle cone. The muscle cone converges at the orbital apex, forming a tendinous ring (annulus of Zinn). Through this ring enters the optic nerve, oculomotor nerve (superior and inferior divisions), abducens nerve, nasociliary branch of the ophthalmic nerve, and the ophthalmic artery. The muscle cone separates the intraconal and extraconal spaces. The contents of these compartments are listed in Table 1.

The globe is continuous with the central nervous system and consists of three distinct layers (Fig 2). From outer to inner, these layers are the sclera, uvea, and retina. The sclera is a collagenous tissue layer that is continuous anteriorly with the cornea and posteriorly with the dura mater. The uvea, or the vascular pigmented layer, consists of the iris, ciliary body, and choroid. The choroid is the most vascular structure of the globe, and thus the most frequent site of intraocular metastases. The retina is light sensitive and continues posteriorly as the optic nerve. Although the layers of the globe cannot be individually identified at routine cross-sectional imaging, they may be visualized in the setting of ocular (choroidal or retinal) detachments.

The bony orbit should be routinely examined in an evaluation of orbital soft-tissue masses. The presence of osseous remodeling generally suggests the diagnosis of a slow-growing process, whereas bone erosion is more suggestive of an aggressive lesion. In addition, the bony foramina, namely the optic canal, superior orbital fissure, and infraorbital canal, carry nerves along which perineural spread or intracranial extension may occur (Fig 3, Table 2).

Table 2
Contents of Orbital Foramina

Foramen	Contents
Superior orbital fissure	Cranial nerves (oculomotor, trochlear, ophthalmic branch of the trigeminal, abducens), superior ophthalmic vein, orbital branch of the middle meningeal artery, sympathetic fibers
Optic canal	Optic nerve, ophthalmic artery, sympathetic fibers
Infraorbital canal	Maxillary branch of the trigeminal nerve, infraorbital artery and vein

Vasculogenic Orbital Masses

Cavernous Malformation

Teaching Point

Although not true neoplasms, cavernous malformations are the most common benign orbital mass in adults. There is much disagreement in the literature about the etiology, classification, and nomenclature of these lesions. Although these masses are commonly referred to as cavernous hemangiomas, many pathologists prefer the term *cavernous malformation*, as the former terminology implies a vasoproliferative neoplasm (2). Cavernous malformations are thought be congenital vascular anomalies that are present at birth, do not spontaneously involute, and grow slowly over time (3).

Patients with cavernous malformations are usually middle-aged adults (mean age, 43–48 years), and there is a female predominance among this patient population. Because these lesions are slow growing, progressive painless proptosis is the most common clinical sign at patient presentation. However, some patients will present with abrupt orbital enlargement and acute-onset proptosis, caused by cytokine and hormonal stimulation at puberty or during pregnancy (3). Approximately half of the patients experience visual field deficits, which are most often from mass effect on the optic nerve or its blood supply (4). Although rare, involvement of the orbital apex can cause compressive optic nerve neuropathy, which leads to monocular vision loss. Other less common symptoms include pain, eyelid swelling, diplopia, or a palpable lump (3).

At microscopy, cavernous malformations appear as dilated cavernous spaces lined by flattened endothelial cells and separated by fibrous septa (Fig 4). A fibrous pseudocapsule surrounds the lesion, giving rise to its well-circumscribed appearance at gross examination. Occasional thrombus or hyalinization may be observed, but calcification is rare (4).

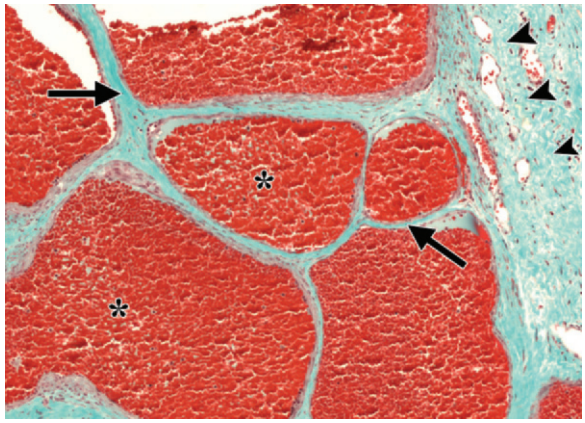

Figure 4. Cavernous malformation. Photomicrograph (original magnification, ×100; Gomori trichrome stain) shows blood-filled spaces (*) separated by collagenous septa (arrows) and surrounded by a fibrous pseudocapsule (arrowheads).

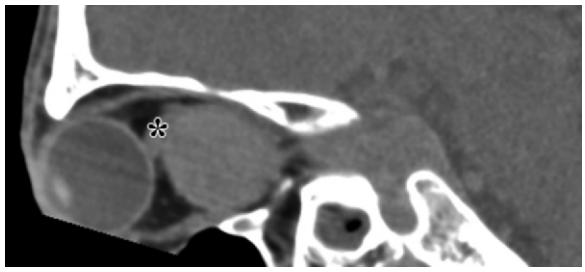

Figure 5. Cavernous malformation in a 46-year-old man with right-sided headache. Sagittal unenhanced CT image demonstrates a round, well-circumscribed intraconal mass that causes superior displacement of the optic nerve (*).

On CT images, cavernous malformations are typically well-circumscribed, homogeneous, and ovoid (Fig 5). The majority of lesions occur at the lateral aspect of the intraconal space (4). Conal and extraconal cavernous malformations are rare. Phleboliths are virtually never seen. Cavernous malformations tend to displace and surround adjacent structures, such as extraconal muscles and the optic nerve, rather than cause direct in-

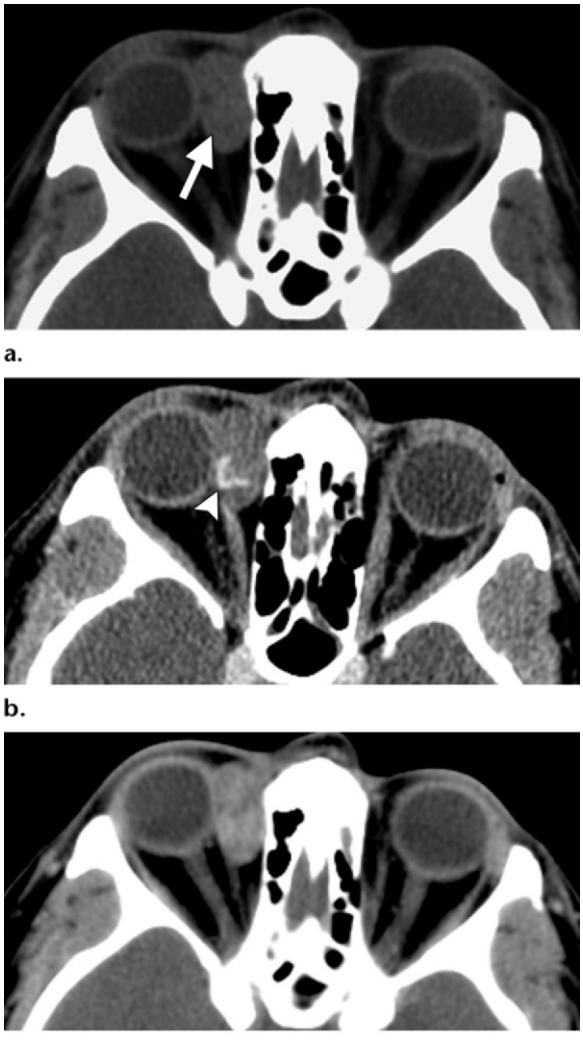

Figure 6. Atypical cavernous malformation in a 44-year-old woman with 1 year of progressive right eye fullness. Multiphase contrast material–enhanced CT was performed. **(a)** Axial nonenhanced image shows a round extraconal mass (arrow). **(b)** Axial arterial phase image shows mild enhancement (arrowhead). **(c)** Axial delayed phase image demonstrates progressive filling. Note that the extraconal location of the mass is atypical for a cavernous malformation.

vasion (5). Osseous remodeling may be present, although bone erosion is rare (5). At magnetic resonance (MR) imaging performed with T1-weighted sequences, cavernous malformations are isointense relative to muscle; the lesions appear uniformly hyperintense on T2-weighted images, with no flow voids. Internal septations may be identified on T2-weighted images (6).

At multiphase CT (Fig 6a, 6b), enhancement of cavernous malformations is poor on early arterial phase images, owing to the scant arterial supply in these lesions (5). Delayed venous phase images demonstrate progressive filling of the mass from periphery to center, with complete filling within 30 minutes (5,7). This enhancement

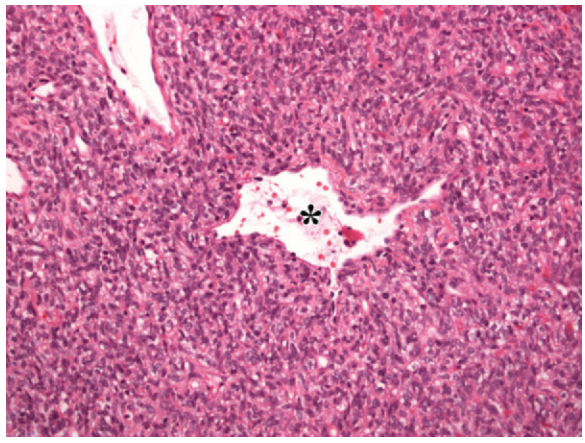

Figure 7. Hemangiopericytoma. Photomicrograph (original magnification, ×200; hematoxylin-eosin stain) shows densely packed spindle cells with a dilated, thin-walled vessel that has a characteristic "staghorn" configuration (*).

pattern may permit differentiation of cavernous malformations from other vascular lesions with rich arterial supply, such as capillary hemangioma (a pediatric diagnosis), hemangiopericytoma, and arteriovenous malformations (3).

Hemangiopericytoma

Hemangiopericytoma is a rare neoplasm, accounting for 1% of all orbital tumors (1). Patients typically present in the 5th decade of life (mean age, 41 years), and the tumor has no gender predilection (8,9). Proptosis and palpable mass are common clinical manifestations. Pain, diplopia, and decreased visual acuity are less common signs (3,8). Hemangiopericytomas range from relatively bland to frankly malignant histologic types, are slow growing, and may recur or metastasize irrespective of histologic type. The metastatic rate of orbital hemangiopericytoma is reported to be 15%, with the lung being the most common site of metastases (8).

Hemangiopericytomas derive from pericytes, the contractile support cells that surround small vessels (9). There is much debate about the pathogenesis and characterization of these tumors (10,11). Many consider the term *hemangiopericytoma* to be a descriptor used to characterize a group of neoplasms with a similar growth pattern. The tumors are thought to have the same cellular lineage as solitary fibrous tumors, and some pathologists believe that many of these lesions are best regarded as solitary fibrous tumors (10,12).

Hemangiopericytoma appears histologically as a dense, hypercellular tumor with spindle-shaped cells (Fig 7). The tumors are vascular with a variably dilated, vascular branching pattern

classically described as "staghorn vessels." Anaplastic features suggestive of a more aggressive neoplasm include increased mitosis, necrosis, infiltrative borders, and cellular pleomorphism (8).

Orbital hemangiopericytomas are typically extraconal, commonly adjacent to the paranasal sinuses. Lesions are usually lobulated and well circumscribed (Fig 8a). Aggressive lesions have infiltrative borders with possible bone erosion (Fig 8b). Calcification is rare. Unlike cavernous malformations, hemangiopericytomas reveal marked arterial enhancement and early venous phase enhancement with rapid washout at multiphase CT. The lesions tend to be isointense relative to gray matter on T1-weighted and T2-weighted images, another feature that may help in differentiating them from cavernous malformation (3).

Lymphoproliferative Lesions

Lymphoproliferative lesions are the most common primary orbital tumor in older adults (≥60 years of age) (13). These lesions represent a spectrum of disorders, including lymphoid hyperplasia, atypical lymphoid hyperplasia, and ocular adnexal lymphoma. Of these, malignant lymphoma is the most common, accounting for 67%–90% of orbital lymphoproliferative tumors and 24% of all space-occupying orbital tumors in patients older than 60 years of age (14). Lesions may be a manifestation of systemic lymphoma or arise primarily from the orbit, with over 30% of patients with solitary orbital lymphoproliferative tumor developing systemic lymphoma 10 years after initial diagnosis (14). Non-Hodgkin lymphoma, specifically the mucosa-associated lymphoid tissue (MALT) subtype, is the most common primary orbital lymphoma (13,15).

Patients typically present with a palpable mass, proptosis, and mildly restricted ocular motility (14). Pain is an uncommon symptom of a lymphoproliferative lesion, in contrast to orbital pseudotumor, which manifests with acute pain (14).

At microscopy, lymphoproliferative lesions may be benign (reactive lymphoid hyperplasia) or malignant (lymphoma). Benign lesions demonstrate well-differentiated, somewhat pleomorphic lymphocytes, whereas malignant lymphoma (Fig 9) demonstrates atypical cells with nuclear membrane abnormalities (15,16). The majority of orbital lymphomas are of B-cell origin. Immunologic markers are particularly valuable for precise diagnosis (16).

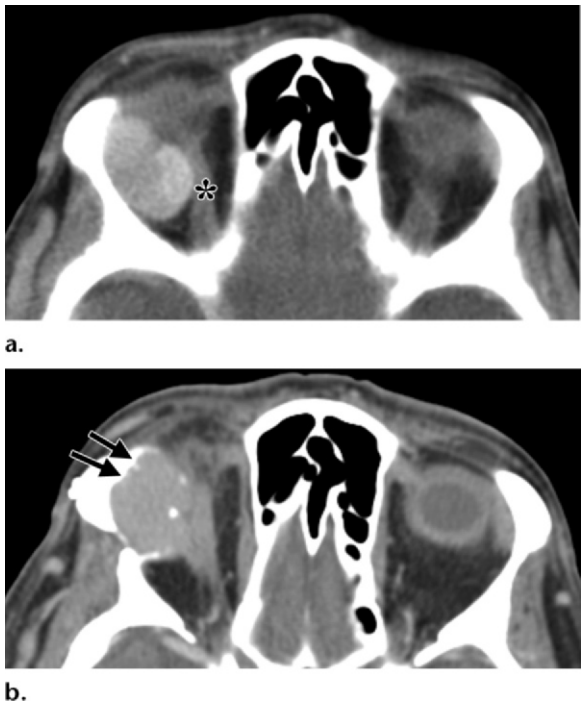

Figure 8. Recurrent hemangiopericytoma in a 64-year-old woman with visual field deficit and diplopia. **(a)** Axial contrast-enhanced CT image shows a lobulated and circumscribed enhancing mass at the superolateral orbit that causes rightward deviation of the superior rectus (*). **(b)** Axial CT image obtained 2 years after resection demonstrates that the lesion has recurred with infiltrative borders and bone erosion (arrows).

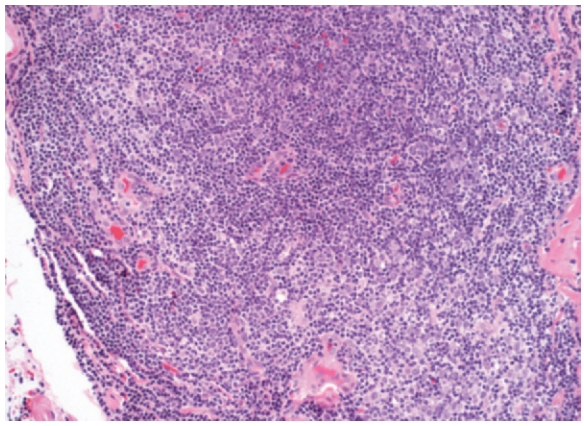

Figure 9. Lymphoma. Photomicrograph (original magnification, ×400; hematoxylin-eosin stain) shows infiltrative lymphocytes in a vague follicular arrangement.

Radiologic examinations do not allow reliable differentiation between benign and malignant

Figure 10. Orbital lymphoma in an 81-year-old man with a history of follicular lymphoma who presented with right eye swelling and proptosis. **(a)** Axial contrast-enhanced CT image shows an ill-defined, enhancing retrobulbar mass that molds to the globe (arrowheads). The optic nerve (*) is encased. **(b)** Coronal CT image shows that the mass has extended through the infraorbital canal (arrow) but without bone erosion.

lymphoproliferative disorders. The majority of lesions are unilateral (76% of cases) and often they are extraconal. The lacrimal gland is involved in nearly 40% of cases (14). At CT or MR imaging, approximately half of the lesions are diffuse and ill defined (Fig 10), with the other half appearing as a smooth, circumscribed mass. Uniform enhancement is characteristic (14,16). One feature of these tumors is their tendency to mold to orbital structures, such as the globe (Fig 10a), optic nerve, and orbital wall; tumor shaped around the latter may result in bone remodeling. Osseous erosion is quite rare, although it may occasionally occur with diffuse large B-cell lymphoma (16). At MR imaging, most lesions are isointense relative to muscle with T1-weighted sequences and hyperintense relative to orbital fat with T2-weighted sequences (17).

Teaching Point

Differentiation of orbital lymphoma from pseudotumor is often challenging at imaging. The findings of infiltration or thickening of ocular muscles favor a diagnosis of pseudotumor (16). One study suggested that pseudotumor is more commonly isointense relative to orbital fat on T2-weighted images (17). In a retrospective study of 47 patients, lymphoma was accurately differentiated from pseudotumor on the basis of apparent diffusion coefficient (ADC) values (18). Review of the patient's clinical history is often useful, since patients with pseudotumor present with a relatively acute onset of pain and those with orbital lymphoma typically have no pain. Ultimately, however, biopsy may be required for diagnosis.

Lacrimal Gland Masses

Lacrimal gland masses represent 5%–14% of biopsied orbital masses. Approximately half of these lesions are benign and half are malignant (19). Masses of the lacrimal gland may be categorized as epithelial or nonepithelial processes. Epithelial lesions compose 40%–50% of lacrimal masses and are largely neoplastic (1,19). Nonepithelial lesions predominantly include inflammatory (dacryoadenitis) and neoplastic (lymphoproliferative disease) processes (20).

Epithelial Lesions

Pleomorphic Adenoma.—Pleomorphic adenoma is the most common benign neoplasm of the lacrimal gland, accounting for up to 57% of epithelial lesions (20). Also called a benign mixed tumor, pleomorphic adenoma contains both mesenchymal and epithelial elements. Pleomorphic adenomas are slow-growing tumors that most often manifest in the 4th or 5th decade of life (21). The lesions commonly displace the globe downward and cause proptosis. Pain is rare and, if present, is suggestive of a different, malignant type of lesion (19).

At histologic analysis, pleomorphic adenoma has a fibrous pseudocapsule with epithelial cells. Cells may form nests or tubules that resemble ducts (Fig 11a). The background stroma may

appear myxoid with spindle-shaped cells and mucin or may contain heterologous elements such as cartilage or bone (15,21).

At CT and MR imaging, pleomorphic adenoma appears as a well-circumscribed, usually homogeneously enhancing mass in the superotemporal orbit. Larger lesions may demonstrate heterogeneity secondary to cystic degeneration, hemorrhage, serous or mucous collections, or necrosis (21). Because of its slow growth, pleomorphic adenoma may demonstrate bone remodeling, which most typically appears as a smooth concavity at the lacrimal fossa (Fig 11b). Lesions are typically hypointense on T1-weighted images and hyperintense on T2-weighted images. Bone erosion is rare and highly suggestive of malignancy. Infiltrative borders and nodularity should also raise suspicion for malignancy (20,21).

Once clinical and imaging diagnosis is established, a pleomorphic adenoma is excised en bloc without biopsy. Incomplete excision or rupture of the tumor may lead to recurrence or malignant transformation to pleomorphic adenocarcinoma. With successful excision, prognosis is excellent (22).

Adenoid Cystic Carcinoma.—Adenoid cystic carcinoma is the most common malignancy of the lacrimal gland and the second most common lacrimal epithelial lesion. It accounts for 29% of all lacrimal epithelial neoplasms and approximately 5% of all primary orbital neoplasms (22). Most patients present in the 4th decade of life. Adenoid cystic carcinoma is infiltrative, with a strong propensity for perineural spread. Owing to this pattern of spread, proptosis may be minimal; however, patients commonly present with pain, which is a strong clinical indicator for malignancy (21). Complete surgical resection may not be possible. Prognosis is generally poor, with a survival rate of 20% at 10 years follow-up (20).

At microscopy, tumors appear nonencapsulated and consist of generally bland-appearing epithelial cells arranged in nests or chords, thus forming a characteristic cribriform (swiss cheese–like) pattern (Fig 12). Unlike pleomorphic adenoma, adenoid cystic carcinoma lacks a mesenchymal matrix (15,21).

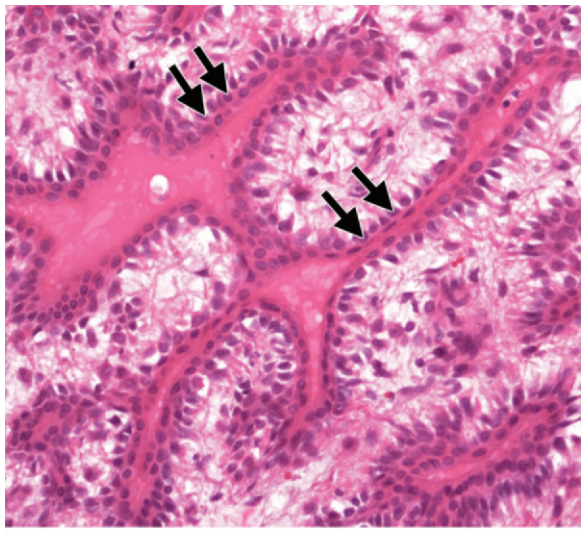

a.

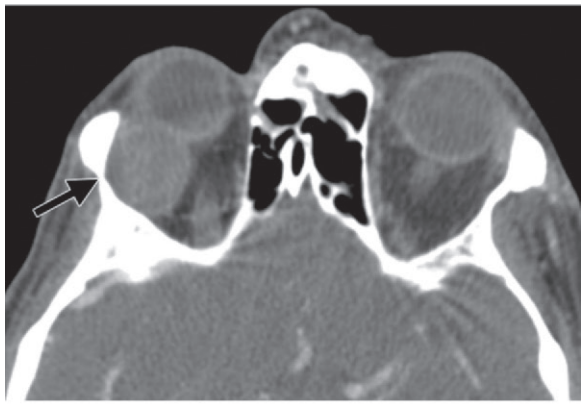

b.

Figure 11. Pleomorphic adenoma. **(a)** Photomicrograph (original magnification, ×200; hematoxylin-eosin stain) shows well-differentiated epithelial cells (arrows) arranged in ductlike tubules. **(b)** Axial contrast-enhanced CT image of a 59-year-old man who presented with right eye dryness shows a homogeneously enhancing, well-circumscribed mass at the lacrimal fossa. Rounded indentation at the zygomatic bone (arrow) reflects bone remodeling caused by slow growth of the tumor.

At imaging, early lesions of adenoid cystic carcinoma may be indistinguishable from pleomorphic adenoma. Irregular borders with distortion of the globe and orbital contents may be seen in patients with more advanced disease (Fig 13). The finding of bone erosion suggests the presence of malignancy, and calcification is

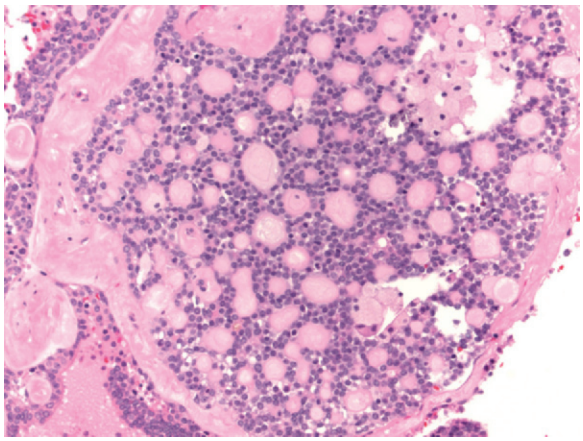

Figure 12. Adenoid cystic carcinoma. Photomicrograph (original magnification, ×200; hematoxylin-eosin stain) shows epithelial tumor cells arranged in nests that form a characteristic swiss cheese–like appearance. The tumor lacks a true capsule.

Figure 13. Adenoid cystic carcinoma in a 53-year-old woman who presented with progressive pain and proptosis. Axial contrast-enhanced CT image shows a heterogeneous extraconal mass at the superolateral orbit with medial displacement of the optic nerve (*) and marked proptosis. There is erosion of the lateral orbital wall (arrowheads) and extension into the temporal fossa (arrow).

also more commonly seen in carcinoma than in benign adenomas (20,21). Cranial nerves, particularly the lacrimal branch of the ophthalmic nerve, should be carefully examined for perineural invasion (20).

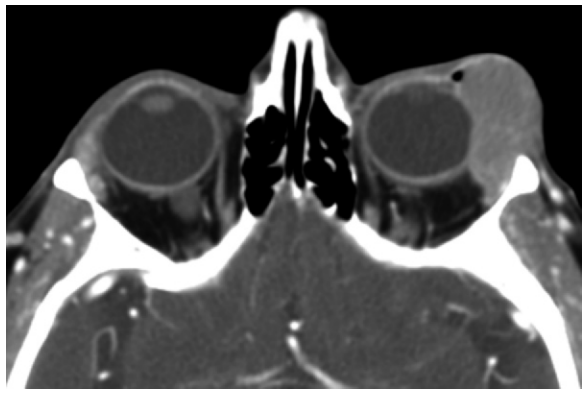

Figure 14. Lacrimal lymphoma in a 76-year-old woman with a palpable mass. Axial contrast-enhanced CT image shows an enhancing lacrimal gland mass, which molds to the globe and does not erode the orbital wall.

Nonepithelial Lesions

Lymphoproliferative disorders constitute up to 50% of nonepithelial lacrimal lesions (19). Malignant lymphoma accounts for the vast majority of these lymphoproliferative processes. Nonetheless, lacrimal lymphoma is quite rare, accounting for only 1% of biopsied orbital masses (1). Most lacrimal gland lymphomas are non-Hodgkin B-cell type (1,23).

Lacrimal gland lymphoma is a disease of older adults, with most patients presenting in the 7th decade of life (mean age, 62–69 years) (1,23). Similar to pleomorphic adenoma, the lesion classically manifests as a painless mass in the superotemporal orbit. Lacrimal gland lymphoma may be associated with Sjögren syndrome. Approximately 35% of patients have or eventually develop systemic lymphoma (19). Prognosis is generally good, with a 5-year survival rate of 70% (23).

At microscopy, lymphoma manifests with small lymphocytes that infiltrate the normal lacrimal glandular tissue. Most lymphomas of the lacrimal gland have low-grade histologic features (23).

At CT, a homogeneously enhancing mass at the lacrimal fossa is usually observed (Fig 14). Bone erosion is typically absent and, if present, suggests an epithelial lesion. Rather than infiltrating orbital contents, lymphoma has a tendency to mold to the

orbit and globe (21,24). The MR imaging signal characteristics of lymphoma are nonspecific (7). Attempts should be made to distinguish lacrimal lymphoma from pleomorphic adenoma, as biopsy of the latter is generally avoided because of the risk of tumor seeding. Older patient age, the presence of lymphadenopathy elsewhere, and lack of osseous remodeling are all characteristics suggestive of lymphoma (24). Lower ADC values may also be indicative of lymphoma, as opposed to other lacrimal gland diseases (25). Other rarer considerations in the differential diagnosis that may mimic tumor include granulomatous diseases, such as sarcoidosis and Wegener granulomatosis, which often have other ocular manifestations not evident at imaging such as uveitis, keratitis, and conjunctivitis (26,27).

Optic Nerve and Meningeal Lesions

Optic Nerve Glioma

Gliomas are the most common primary tumor of the optic nerve (1). They may occur anywhere along the optic tract; 25%–48% are confined to the intraorbital optic nerve (7). Nearly all optic nerve gliomas are juvenile pilocytic astrocytomas (grade 1 as defined by the World Health Organization) and manifest in children less than 8 years of age. Gliomas are associated with neurofibromatosis type 1 (NF-1), with 20% of children with NF-1 having optic nerve gliomas, often with bilateral involvement (7,28). Although extremely rare, malignant optic nerve gliomas may occur in adults. Such malignant lesions are aggressive, are not associated with NF-1, and are classified as anaplastic astrocytoma or glioblastoma multiforme.

Optic nerve gliomas may be asymptomatic and discovered incidentally in patients with NF-1, or patients may present with a visual field deficit, vision loss strabismus, or relative afferent pupillary defect. Treatment is generally reserved for cases with documented progression (28).

At histologic analysis, juvenile pilocytic astrocytomas consist of spindle-shaped astrocytes with hairlike (pilocytic) processes. Eosinophilic degenerative cell processes, called Rosenthal fibers, may be present (Fig 15). The leptomeninges show reactive hyperplasia and cellular infiltration; however, the dura mater remains intact, resulting in fusiform or sausage-shaped nerve expansion.

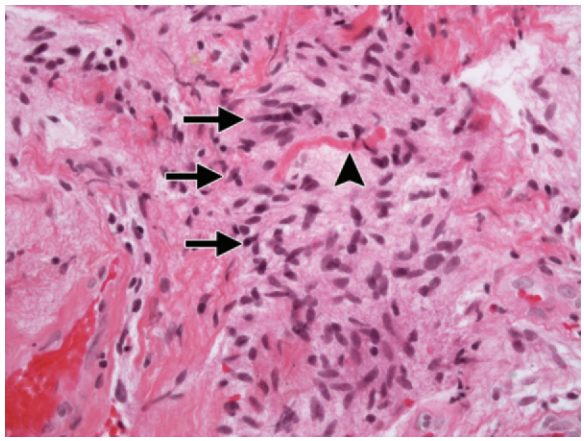

Figure 15. Optic nerve glioma. Photomicrograph (original magnification, ×400; hematoxylin-eosin stain) shows elongated spindle cells (arrows) with Rosenthal fibers (arrowhead). Histologic characteristics are compatible with pilocytic astrocytoma.

Malignant optic nerve gliomas show high mitotic activity, necrosis, and hemorrhage (15).

The imaging appearance of optic nerve gliomas is characteristic, such that biopsy is rarely performed (1) (Fig 16). MR imaging is the modality of choice, particularly for assessing involvement of the orbital apex, optic chiasm, hypothalamus, and other intracranial structures (28). The lesions are typically isointense on T1-weighted images and isointense to hyperintense on T2-weighted images. Enhancement is variable, and cystic spaces may be seen. Calcifications are rare (7). A rim of T2 hyperintensity is often observed at the tumor periphery, a finding that may mimic an expanded subarachnoid space (Fig 16a). However, this finding corresponds histopathologically to leptomeningeal infiltration and proliferation (so-called arachnoidal gliomatosis) (28).

The appearance of optic nerve gliomas is different in patients with and without NF-1. In patients with NF-1, the optic nerve often appears tortuous, kinked or buckled, and diffusely enlarged (Fig 17). In patients without NF-1, gliomas tend to be fusiform. Isolated chiasmal gliomas are more likely in the absence of neurofibromatosis, and chiasmal involvement is also more common in patients who do not have neurofibromatosis (29). At imaging, the nerve itself cannot be distinguished from the tumor, a characteristic that is useful for differentiating glioma from meningioma (7).

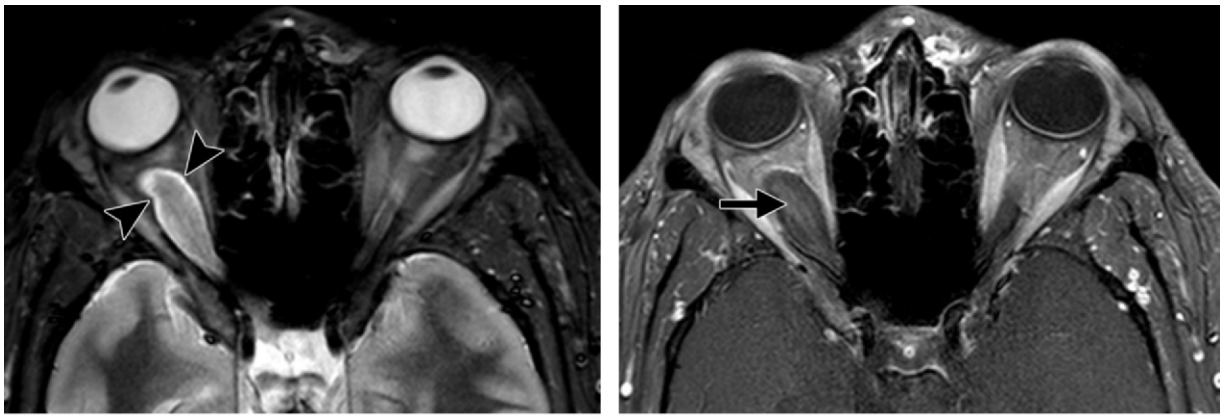

a. b.

Figure 16. Optic nerve glioma in a 6-year-old girl with proptosis. **(a)** Axial short inversion time inversion-recovery MR image shows an expansile mass that involves the right optic nerve. The hyperintense rim at the tumor periphery (arrowheads) reflects leptomeningeal infiltration. **(b)** Axial postcontrast T1-weighted fat-suppressed image shows minimal enhancement in the mass (arrow). The nerve itself cannot be separated from the tumor.

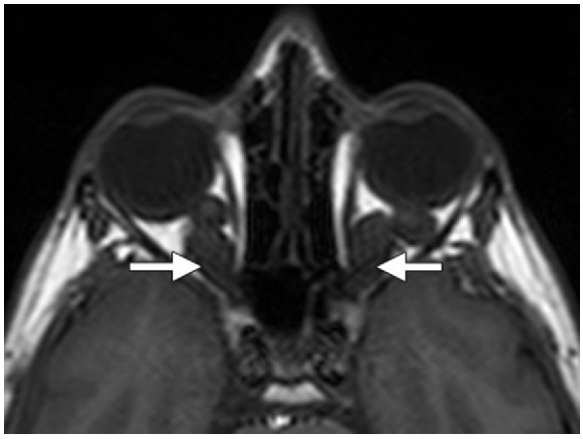

Figure 17. Bilateral optic nerve gliomas in a 25-year-old man with NF-1. Axial T1-weighted image shows the tortuous and kinked appearance of the bilateral optic nerves (arrows).

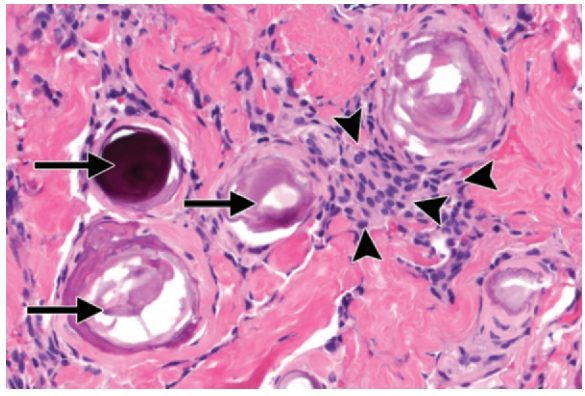

Figure 18. Meningioma. Photomicrograph (original magnification, ×200; hematoxylin-eosin stain) shows meningioma cells with indistinct borders (arrowheads) and multiple ringlike psammoma bodies (arrows).

Optic Nerve Sheath Meningioma

Optic nerve sheath meningiomas derive from the arachnoid sheath of the optic nerve. They are the second most common optic nerve tumor, accounting for 2% of space-occupying orbital masses (1). Primary optic nerve meningiomas are less frequent than secondary lesions that extend into the orbit from an intracranial site (15). As with optic nerve gliomas, cross-sectional imaging features are characteristic, such that biopsy is usually not warranted (1). As with intracranial meningiomas, optic nerve sheath meningiomas are more common in women. Patients usually present in the 5th decade of life (mean age, 48–50 years) (1,30). The classic clinical triad includes painless, slowly progressive loss of vision; optic nerve atrophy; and the presence of optociliary shunt vessels, which result after long-term compression of the central retinal vein (30).

Histologic analysis often shows a syncytial growth pattern, composed of cells with indistinct cytoplasmic margins (Fig 18). Psammoma bodies (round calcifications surrounded by meningioma cells) may be present (15,30).

Similar to optic nerve gliomas, optic nerve sheath meningiomas may appear as an expansion of the optic nerve. However, because the substance of the nerve is spared, a "tram-track" configuration is often observed at axial contrast-enhanced CT or MR imaging, since enhancing tumor lies on either side of the nerve (Fig 19). On coronal images, this configuration appears similar to a donut (31). Aside from this classic tubular growth pattern, meningiomas may also manifest as a fusiform or eccentric mass. Contrast-enhanced MR imaging is

Teaching Point

the study of choice for evaluation, particularly for its value in determining the extent of disease (Fig 20). T1 and T2 signal characteristics are variable (30). CT better shows bone remodeling and calcification, the latter of which occurs in 20%–50% of cases (7,30).

With all tumors of the optic nerve or optic nerve sheath, including gliomas and meningiomas, it is important to define the extent of disease involvement and document any evidence of disease progression. Clinicians and surgeons must know precisely which portions of the optic nerve tract (intraoptic, intracanalicular, and intracranial) are involved with disease (Fig 20). Optic nerve tumors, including meningiomas in adults and optic nerve gliomas in children, are generally slow growing and, therefore, may not require frequent follow-up. Conversely, optic nerve sheath meningiomas in children and optic nerve gliomas in adults may be aggressive. Therefore, it is important to closely monitor the extent of involvement. If disease is spreading to approximate the optic chiasm, surgical intervention may be warranted to prevent disease dissemination to the contralateral eye (32).

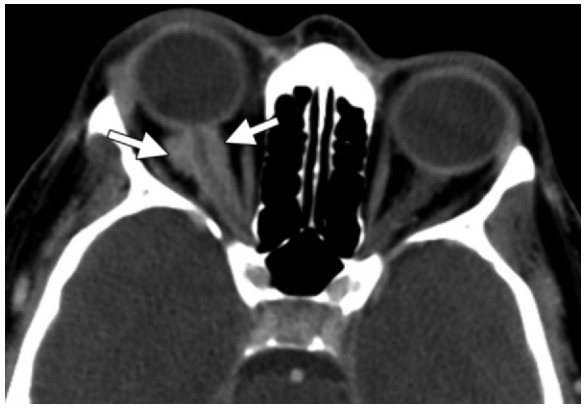

Figure 19. Optic nerve sheath meningioma incidentally found in a 50-year-old woman. Axial contrast-enhanced CT image demonstrates the tram-track configuration of an enhancing tumor (arrows) surrounding the optic nerve. The mass extends to the orbital apex. The optic nerve itself can be separated from the tumor.

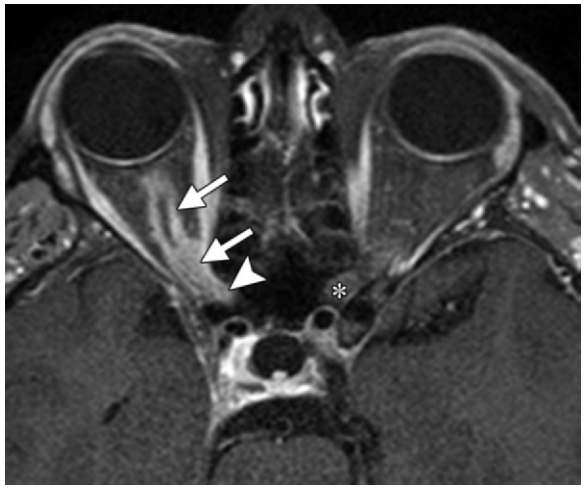

Figure 20. Optic nerve sheath meningioma in a 62-year-old patient who presented with blurry vision of the right eye. Axial contrast-enhanced T1-weighted fat-suppressed MR image demonstrates an avidly enhancing tumor along both sides of the right optic nerve. The intraoptic and intracanalicular portions of the optic nerve are involved (arrows), as well as the prechiasmatic portion of the intracranial optic nerve (arrowhead). ∗ = normal left intracranial optic nerve.

Peripheral Nerve Sheath Lesions

Schwannoma

Schwannomas (also called neurilemomas) are encapsulated, slowly progressive, benign proliferations of Schwann cells (33). They form as eccentric growths (eg, acoustic neuroma) from any peripheral nerve, most commonly from the vestibulocochlear nerve. Schwannomas are rare in the orbit, most commonly arising from branches of the trigeminal nerve; however, they may arise from peripheral branches of the oculomotor, trochlear, and abducens nerves; parasympathetic and sympathetic fibers; and the ciliary ganglia (1,6).

Schwannomas tend to occur in middle-aged individuals; however, they are seen in patients of a wide range of ages (20–70 years) (34). Clinical symptoms are nonspecific and can be similar to those manifested by patients with cavernous malformation, making preoperative ophthalmologic diagnosis difficult. Perineural spread may result in progressive symptoms, pain, and neural compression. Hence, surgical resection is the treatment of choice (6).

Two distinct patterns are seen at microscopy (Fig 21). The Antoni A pattern is cellular, composed of spindle cells arranged in fascicles or chords that may form Verocay bodies (pallisading arrangements of elongated cells) (15). The Antoni B pattern is a looser arrangement of stellate cells in a mucoid stroma (33). Both patterns often coexist in a single tumor.

Schwannomas are typically extraconal and located at the superior orbit, owing to their frequent origin from the frontal branch of the ophthalmic nerve, which further divides into the supratrochlear and supraorbital nerves (34). The lesions often abut orbital apertures, assuming a cone shape if the orbital apex is involved or a dumbbell shape when the superior orbital fissure is involved (33).

MR imaging is superior to CT in the evaluation of schwannomas, and it facilitates preopera-

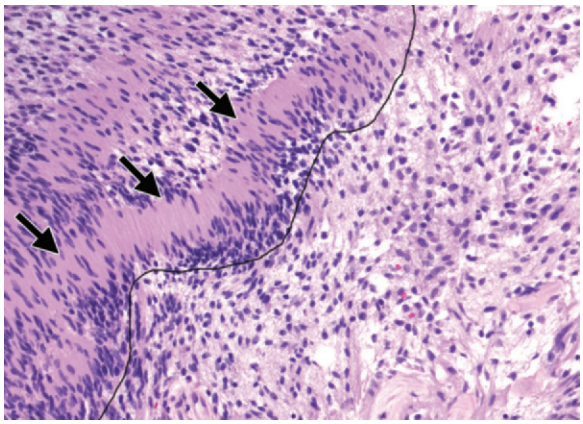

Figure 21. Schwannoma. Photomicrograph (original magnification, ×100; hematoxylin-eosin stain) shows the cellular Antoni A pattern with Verocay bodies (arrows) in the top left, whereas the loosely arranged Antoni B pattern is seen in the bottom right.

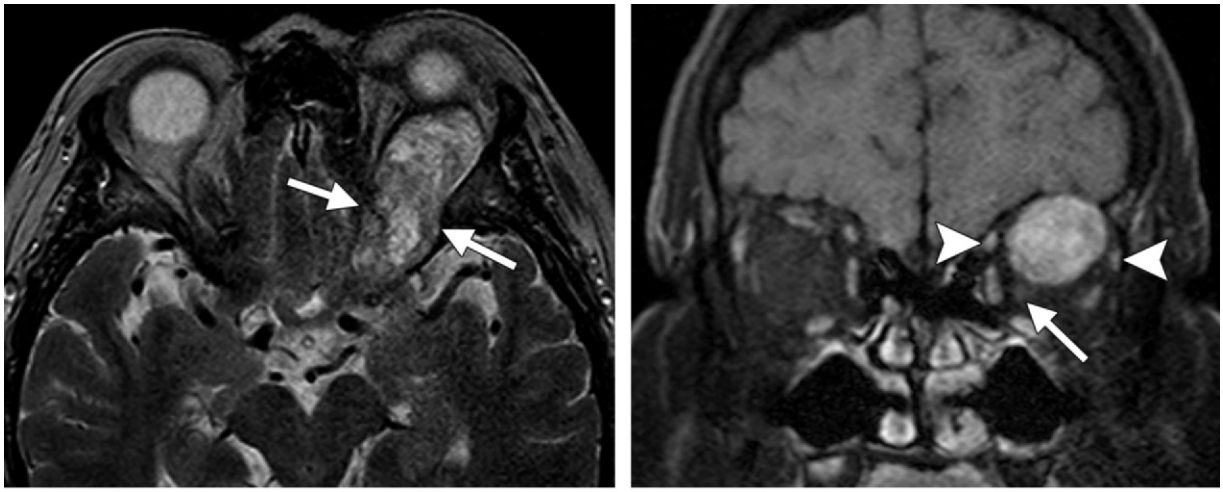

a. b.

Figure 22. Schwannoma in a 56-year-old woman with progressive proptosis and decreased eye movements. **(a)** Axial T2-weighted MR image shows a heterogeneously hyperintense mass that expands the superior orbital fissure (arrows). **(b)** Coronal postcontrast T1-weighted fat-suppressed MR image shows heterogeneous enhancement of the mass. The tumor splays apart the superior oblique and superior rectus muscles (arrowheads) and causes downward displacement of the optic nerve (arrow).

tive planning by revealing the exact location and extent of disease. MR imaging features may be helpful in differentiating a schwannoma from a cavernous malformation (6,33). In addition, T2 signal characteristics and contrast enhancement patterns may provide histopathologic information (33). On T1-weighted images, a schwannoma typically appears as a uniformly isointense, well-circumscribed mass, although this appearance is nonspecific and variable. Schwannomas are usually T2 hyperintense, although heterogeneous, a pattern that differs from the relatively homogeneous pattern of cavernous malformations (6) (Fig 22). This heterogeneity likely reflects the mixed solid and cystic components of the tumor, as well underlying Antoni A and B cellular patterns. Schwannomas of the Antoni B histologic type tend to appear with T2 hyperintensity, whereas those of the Antoni A type tend toward T2 hypointensity with contrast material uptake (33). After intravenous contrast material administration, heterogeneous uptake is typically observed (Fig 22b). Progressive enhancement on delayed venous phase images favors a diagnosis of cavernous malformation over schwannoma (6,7).

Neurofibroma

Neurofibromas are benign, slow-growing, peripheral nerve tumors composed of an admixture of fibroblasts, Schwann cells, and axons (15). Localized, diffuse, and plexiform types may occur in the orbit. Amputation (traumatic) neuromas may also occur in patients with a history of prior surgery, such as enucleation, although these tumors are extremely rare (35).

Plexiform neurofibromas are the most common type of peripheral nerve sheath tumor and are essentially pathognomonic for NF-1. Diffuse types of neurofibroma have a more variable association with NF-1. Solitary orbital neurofibromas

Figure 23. Neurofibromas in a 35-year-old man with NF-1. Coronal fluid-attenuated inversion-recovery MR images demonstrate multiple hyperintense extraconal masses, one at the superior orbit (arrows in **a**) and one located in the infraorbital canal, involving the V2 division of the trigeminal nerve (ie, the maxillary nerve) (arrowhead in **b**).

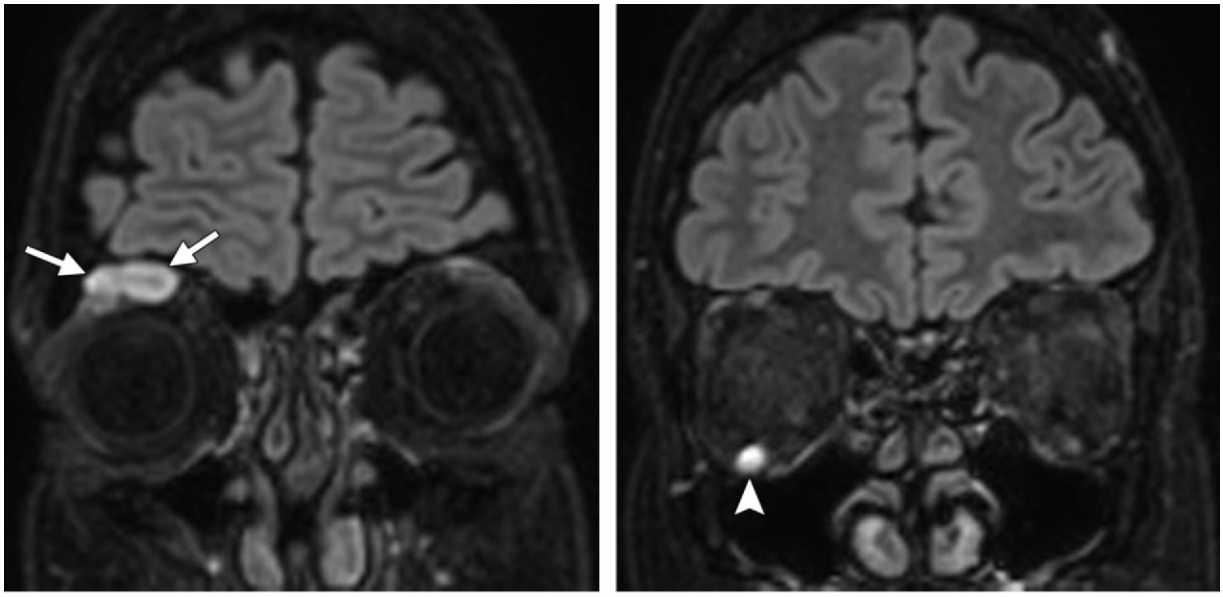

a. **b.**

are quite rare (36). In one series of 1264 patients with orbital tumors, only two patients (<1%) were found to have solitary neurofibroma (1). The solitary form is associated with neurofibromatosis in approximately 12% of cases (36).

Histologic analysis reveals spindle-shaped cells arranged in ribbons and cords among a background of loose myxoid stroma. The majority of neurofibromas are benign, lacking cellular atypia. Solitary subtypes are well circumscribed, although unlike schwannomas, neurofibromas lack a capsule (15).

Similar to schwannomas, neurofibromas are more commonly extraconal, owing to their frequent origin from sensory branches of the trigeminal nerve (36) (Fig 23). On cross-sectional images, plexiform neurofibromas appear as serpentine soft-tissue masses with heterogeneous uptake of contrast material. They are typically hyperintense on T2-weighted images and heterogeneous in intensity on T1-weighted images. The lesions may cross tissue planes and involve large portions of the face. At clinical and imaging examinations, the appearance of plexiform neurofibromas is often compared with that of a "bag of worms." The tendency of these lesions to insinuate between tissue planes is also characteristic of lymphatic malformations; however, the latter demonstrate fluid-fluid levels, best seen at MR imaging, an appearance highly suggestive of the diagnosis (37).

Clinical and imaging features of solitary neurofibroma are largely indistinguishable from those of schwannoma. As with schwannoma, solitary neurofibromas often occur at the superior extraconal orbit, causing downward displacement of the globe (hypoglobus). However, because it lacks a capsule, the borders of a solitary neurofibroma may be less well defined than those of a schwannoma (7). Cystic components and T2 heterogeneity may suggest the diagnosis of a schwannoma (36). Most often, the distinction between these two entities is not possible at imaging, which is somewhat of a moot point as both are readily amenable to surgical excision. The primary reason for attempting to differentiate between these lesions is that malignant transformation, although rare, is believed to be more common with neurofibroma (38). Patient history may be particularly helpful in suggesting a diagnosis, since neurofibroma is the hallmark lesion of NF-1 and schwannoma is more characteristic of NF-2 (39). In the absence of such history, the final diagnosis lies with the pathologist.

Malignant Peripheral Nerve Sheath Tumor

Malignant peripheral nerve sheath tumors may arise de novo or from preexisting peripheral nerve sheath tumors. They most commonly affect the sciatic nerve and are rare in craniofacial and orbital locations (40). The lesions are sarcomas and often lack a single tissue of origin at histologic analysis. Patients with NF-1 carry a 10% lifetime risk of developing malignant peripheral nerve sheath tumors, which most commonly arise from plexiform neurofibromas (39). Clinical and radiologic features of malignant tumor may be

Figure 24. Choroidal melanoma. **(a)** Diagram illustrates how a melanotic lesion causes retinal detachment. As melanoma breaks through the choroid, it separates the retina from the choroid. **(b)** Photograph of a gross specimen from enucleation demonstrates a large mass (arrows) that nearly fills the vitreous chamber. The retina is detached in many areas (arrowheads). **(c)** Photomicrograph (original magnification, ×100; hematoxylin-eosin stain) shows epithelioid-type choroidal melanoma cells (black double arrow) adjacent to the sclera (white double arrow). A nest of melanoma cells (single arrows) invades the sclera.

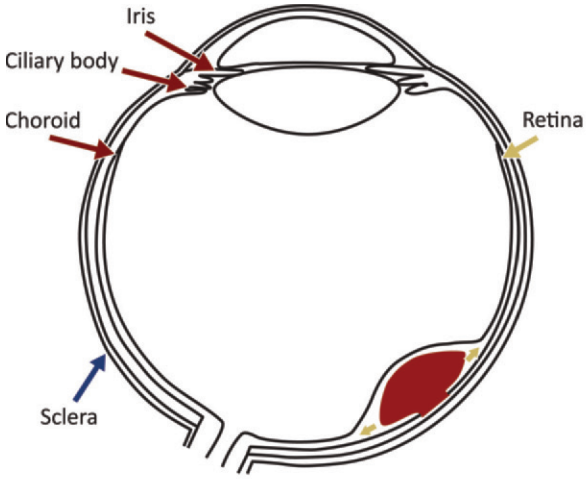

a.

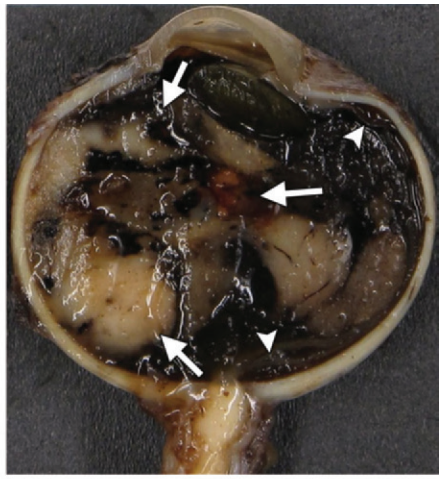

b.

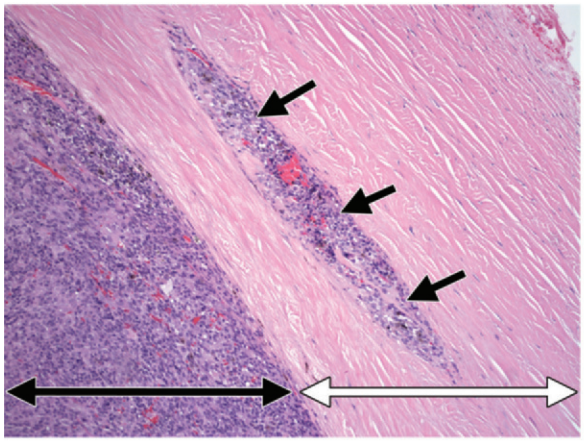

c.

indistinguishable from those of a benign peripheral nerve sheath tumor. Comparison with prior examinations is valuable, with rapid growth and soft-tissue or bone destruction being highly suggestive of malignancy (38,39).

Primary Melanocytic Neoplasms

Primary orbital melanoma is the most common primary intraocular malignancy in adults. It is far more common among Caucasians (41). Other risk factors include a light-colored iris and ocular melanocytosis. Patients usually present in the 6th decade of life (mean age, 56 years); there is no gender predominance among this group of neoplasms. Unlike the risk factors for cutaneous melanoma, the relationship of ultraviolet light exposure to the development of uveal melanoma is unclear (42).

Orbital melanoma arises from the uveal tract, which consists of the choroid, ciliary body, and iris. The majority of lesions (90%) derive from the choroid (41). Iris melanomas follow a relatively nonaggressive course, whereas ciliary body and choroidal melanomas portend a far worse prognosis (43). Because of their visible location, iris melanomas are typically diagnosed and treated with surgical resection early on and are not routinely imaged (42).

In contrast to patients with iris melanomas, approximately half of patients with choroidal melanomas die of metastatic disease. The liver is the most common site of metastases and is involved in up to 90% of patients with metastatic disease (41). Extrahepatic sites of metastases include the lung, bone, and skin (3). Treatment of choroidal melanomas depends on lesion size, with larger lesions usually treated with enucleation and smaller lesions managed with eye-conserving therapies (44). Therapeutic options for metastatic disease are limited (41).

Choroidal melanomas may be asymptomatic, or patients may present with decreased vision, visual field defects, or floaters. Pain is uncommon (42). As lesions grow, they expand the choroid and rupture through the Bruch membrane (innermost layer of the choroid), assuming a characteristic mushroom shape. Continued expansion of the tumor results in retinal detachment in most cases (Fig 24a, 24b). Less commonly, curvilinear growth occurs along the choroid (15). Tumor cells may

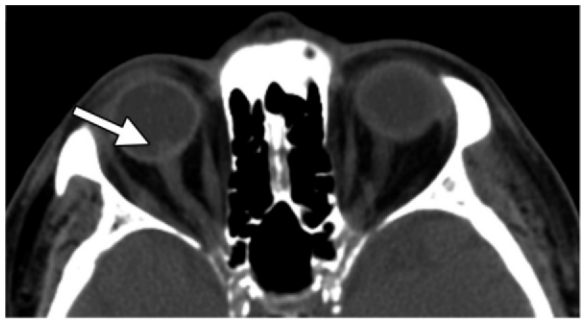

25.

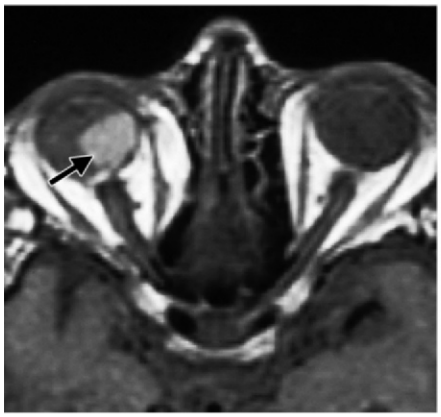

26a.

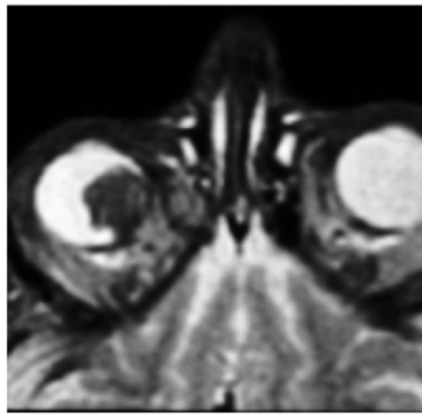

26b.

Figures 25, 26. **(25)** Choroidal melanoma discovered at fundoscopy in a 55-year-old woman. Axial contrast-enhanced CT image demonstrates a subtle enhancing nodule at the level of the optic disk (arrow). **(26)** Choroidal melanoma. **(a)** Axial T1-weighted image shows a rounded hyperintense mass (arrow) in the right posterior globe. **(b)** On an axial T2-weighted image, the lesion appears hypointense.

also infiltrate the underlying sclera, resulting in episcleral spread (Fig 24c).

Choroidal melanomas consist of spindle cells or epithelioid cells. Unlike nevi, which more frequently contain spindle-A cells, choroidal melanomas contain varying amounts of spindle-B cells, which have higher nuclear-to-cytoplasmic ratio and more prominent nucleoli. Epithelioid cells have abundant cytoplasm, clear cellular borders, and enlarged ovoid nuclei (15,41) (Fig 24c).

Diagnosis is typically made at fundoscopy; however, imaging studies are valuable for identifying disease extent (42). CT is nonspecific, often demonstrating a hyperattenuating choroidal mass (Fig 25). MR imaging is superior to CT in the evaluation of choroidal melanomas, as melanin has intrinsic T1 and T2 shortening effects, thereby manifesting with increased T1 signal intensity and decreased T2 signal intensity (3,45) (Fig 26). Studies have shown that the degree of melanomatous pigmentation correlates with quantitative T1 signal (46). This finding may be of value in predicting patient prognosis, as strong pigmentation confers a less favorable prognosis. MR imaging is also valuable for identifying other features, such as large tumor size, extraocular extension, and ciliary body infiltration, all of which also portend a poorer prognosis (46). In addition, MR imaging is superior to CT for identifying retinal detachment and extrascleral spread (45).

Teaching Point

Notably, approximately 20% of melanomas are amelanotic, thereby lacking characteristic T1 and T2 shortening effects on MR images (46). In addition, MR signal characteristics may not always allow melanoma to be reliably distinguished from ocular metastases (47).

Metastatic Lesions

Metastases from other cancers constitute 1%–13% of orbital tumors (1). Metastatic breast cancer is the most common type to metastasize to the orbit, accounting for 48%–53% of orbital metastases, followed by metastatic prostate carcinoma, melanoma, and lung cancer (48,49) (Figs 27–29). Metastases to the globe most frequently involve the choroid, with metastatic lung cancer being most commonly implicated (50).

Teaching Point

Clinical symptoms generally manifest rapidly, with progression occurring over weeks to months (51). Proptosis and motility disturbances are among the most common presenting signs. Pain, diplopia, and decreased vision are also not infrequent. A less common, and often overlooked sign, is paradoxical enophthalmos, which is observed in 10% of metastatic orbital lesions (52). Paradoxical enophthalmos is most often a sequela of scirrhous breast cancer, which produces infiltrative and

Figures 27–29. **(27)** Breast cancer metastasis in a 56-year-old woman who presented with eye pain. Axial postcontrast T1-weighted fat-suppressed MR image shows thickening of the left lateral rectus muscle (arrows), with involvement of the tendinous insertion. Biopsy results revealed breast cancer, which was undiagnosed at presentation. **(28)** Metastatic scirrhous breast cancer in a 43-year-old woman with bilateral paradoxical enophthalmos. **(a)** Axial T1-weighted image shows abnormally hypointense and heterogeneous bilateral retrobulbar fat (arrows). **(b)** Axial postcontrast T1-weighted fat-suppressed image shows patchy enhancement of the retrobulbar fat (arrows). The left medial rectus is also thickened because of metastatic involvement (arrowhead). **(29)** Melanoma metastatic to the extraocular muscle in a 37-year-old man who presented with decreased vision. **(a)** Axial T1-weighted image shows a mass of the inferior rectus muscle that appears isointense (arrow), reflecting its amelanotic nature. **(b)** Photograph of a gross specimen from the same patient shows diffuse enlargement of the inferior rectus muscle (arrow).

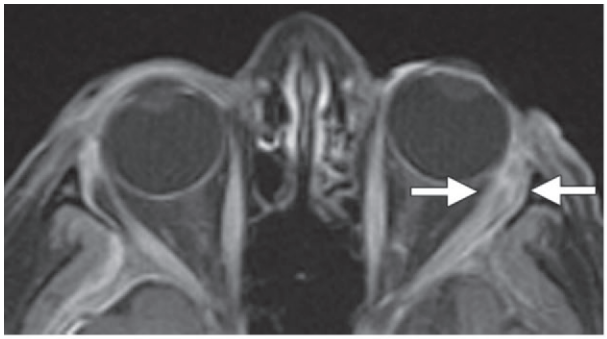

27.

29a.

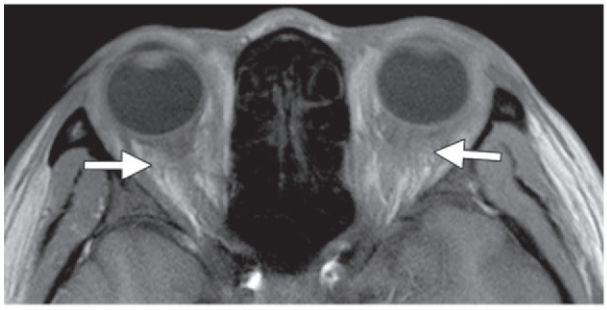

28a.

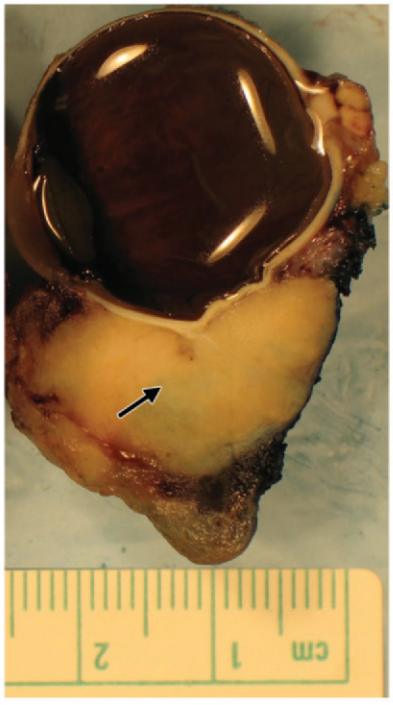

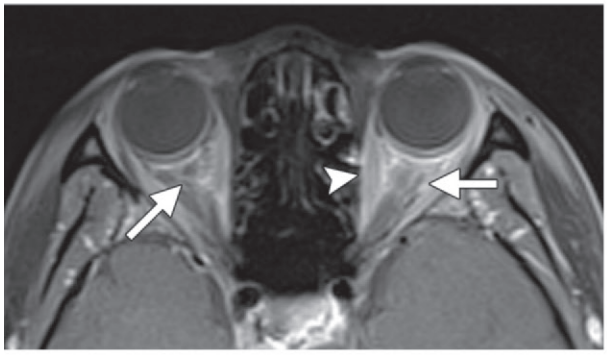

28b.

29b.

fibrotic contraction of orbital fat, leading to posterior globe retraction (52,53). On T1-weighted and T2-weighted MR images, the retrobulbar fat demonstrates diffuse enhancement with abnormally heterogeneous hypointensity, reflective of fibrotic infiltration (Fig 28). In rare cases, this pattern may also be observed with metastatic scirrhous gastrointestinal carcinomas (52).

Differentiating orbital metastasis from nonneoplastic infiltrative processes may pose a diagnostic challenge. For conal metastasis in particular, differential diagnostic considerations include thyroid ophthalmopathy, which is often bilateral and spares tendinous insertions, as well as orbital pseudotumor, which is typically painful and may be differentiated from thyroid ophthalmopathy because pseudotumor involves the tendinous insertion. Granulomatous disease, such as sarcoidosis,

Table 3
Summary of Orbital Neoplasms

Diagnosis by Histologic Category	Location	Characteristic Imaging Findings
Vasculogenic		
Cavernous malformation	Intraconal more often than extraconal	Well-circumscribed, homogeneous ovoid mass; poor arterial enhancement, progressive filling on delayed phase images
Hemangiopericytoma	Extraconal more often than intraconal	Low-grade lesions are lobulated and well circumscribed; aggressive features include infiltrative borders and osseous erosion; marked arterial phase enhancement with rapid washout
Lymphoproliferative		
Lymphoid hyperplasia, atypical hyperplasia, lymphoma	Extraconal more often than intraconal	Benign and malignant lesions cannot be distinguished reliably at imaging; lesions may be smooth and well circumscribed or diffuse and ill defined; enhancement is uniform; lesions mold to orbital structures; osseous erosion is rare
Lacrimal gland		
Pleomorphic adenoma	Extraconal	Well-circumscribed mass with homogeneous enhancement; osseous remodeling is common; osseous erosion is rare and suggests alternate malignant diagnosis
Adenoid cystic carcinoma	Extraconal	Early lesions appear identical to pleomorphic adenoma; irregular borders with distortion of orbital contents; osseous erosion may be present; tendency for perineural spread
Lacrimal gland lymphoma	Extraconal	Homogeneously enhancing round mass; osseous erosion is rare
Optic nerve and meningeal		
Optic nerve glioma	Intraconal with or without intracranial involvement	Fusiform enlargement of the optic nerve; tortuous or kinked optic nerve in NF-1 patients
Optic nerve sheath meningioma	Intraconal with or without intracranial involvement	Enhancing tumor with tram-track configuration on axial contrast-enhanced CT or MR images; possible bone remodeling and calcification
Peripheral nerve sheath		
Schwannoma	Extraconal more often than intraconal; often in superior orbit	Mixed solid and cystic mass with heterogeneous enhancement; dumbbell shaped if superior orbital fissure is involved; cone shaped if orbital apex is involved
Neurofibroma	Extraconal more often than intraconal; may be localized, diffuse, or plexiform	Plexiform types may involve large portions of the face with a bag-of-worms appearance; solitary types difficult to distinguish from schwannoma
Primary melanocytic		
Primary orbital melanoma	Globe (choroid is most common site)	Enhancing nodule or mass arising from the choroid; retinal detachment; possible extrascleral spread
Metastatic		
Most common types include metastases from breast cancer, prostate cancer, melanoma, lung cancer	Globe, intraconal, extraconal, or muscle cone	Breast cancer has tendency for orbital fat and muscle lesions; prostate cancer has tendency for bone lesions; melanoma has strong preference for muscle lesions; scirrhous breast cancer causes enophthalmos with heterogeneously enhancing retrobulbar fat

may also mimic metastatic disease and can involve the extraocular muscles, optic nerve, optic chiasm, or lacrimal gland (21,54).

At imaging, it may be difficult to establish a principal tissue site of metastasis because by the time of radiologic evaluation, disease may have infiltrated orbital muscles, fat, and bone. However, different malignancies have tendencies toward localizing to certain tissues. Breast cancer has a tendency to localize to orbital fat and muscle, prostate cancer has a tendency to disseminate to bone, and melanoma has strong preference for muscle (52). Knowledge of these general trends can be useful for the radiologist in constructing a differential diagnosis and may also guide work-up in cases in which a primary tumor is not yet established.

Conclusions

Cross-sectional imaging can aid in the diagnosis and evaluation of orbital neoplasms, supplementing findings from fundoscopic and clinical ophthalmologic examinations. A compartmental approach to assessing orbital disease, with a consideration of histologic composition, guides the differential diagnostic considerations for this complex group of diseases (Table 3). Use of MR imaging is especially valuable for assessing the extent of disease. Precise descriptions of lesion location, involved orbital compartments, spread to the orbital apex or along perineural pathways, and associated intracranial abnormalities provide information beyond what can be seen at fundoscopy and facilitate appropriate treatment.

References

1. Shields JA, Shields CL, Scartozzi R. Survey of 1264 patients with orbital tumors and simulating lesions: the 2002 Montgomery Lecture, part 1. Ophthalmology 2004;111(5):997–1008.
2. Lowe LH, Marchant TC, Rivard DC, Scherbel AJ. Vascular malformations: classification and terminology the radiologist needs to know. Semin Roentgenol 2012;47(2):106–117.
3. Smoker WR, Gentry LR, Yee NK, Reede DL, Nerad JA. Vascular lesions of the orbit: more than meets the eye. RadioGraphics 2008;28(1):185–204.
4. Harris GJ, Jakobiec FA. Cavernous hemangioma of the orbit. J Neurosurg 1979;51(2):219–228.
5. Ansari SA, Mafee MF. Orbital cavernous hemangioma: role of imaging. Neuroimaging Clin N Am 2005;15(1):137–158.
6. Wang Y, Xiao LH. Orbital schwannomas: findings from magnetic resonance imaging in 62 cases. Eye (Lond) 2008;22(8):1034–1039.
7. Yousem DM, Zimmerman RD, Grossman RI. Neuroradiology: the requisites. Philadelphia, Pa: Mosby, 2010.
8. Croxatto JO, Font RL. Hemangiopericytoma of the orbit: a clinicopathologic study of 30 cases. Hum Pathol 1982;13(3):210–218.
9. Ruchman MC, Flanagan J. Cavernous hemangiomas of the orbit. Ophthalmology 1983;90(11):1328–1336.
10. Gengler C, Guillou L. Solitary fibrous tumour and haemangiopericytoma: evolution of a concept. Histopathology 2006;48(1):63–74.
11. Park MS, Araujo DM. New insights into the hemangiopericytoma/solitary fibrous tumor spectrum of tumors. Curr Opin Oncol 2009; 21(4):327–331.
12. Goldsmith JD, van de Rijn M, Syed N. Orbital hemangiopericytoma and solitary fibrous tumor: a morphologic continuum. Int J Surg Pathol 2001; 9(4):295–302.
13. Demirci H, Shields CL, Shields JA, Honavar SG, Mercado GJ, Tovilla JC. Orbital tumors in the older adult population. Ophthalmology 2002;109 (2):243–248.
14. Demirci H, Shields CL, Karatza EC, Shields JA. Orbital lymphoproliferative tumors: analysis of clinical features and systemic involvement in 160 cases. Ophthalmology 2008;115(9):1626–1631, 1631.e1–e3.
15. Rosa RH, Buggage R, Harocopos GJ, et al. Ophthalmic pathology and intraocular tumors. San Francisco, Calif: American Academy of Ophthalmology, 2011.
16. Valvassori GE, Sabnis SS, Mafee RF, Brown MS, Putterman A. Imaging of orbital lymphoproliferative disorders. Radiol Clin North Am 1999;37(1): 135–150.
17. Cytryn AS, Putterman AM, Schneck GL, Beckman E, Valvassori GE. Predictability of magnetic resonance imaging in differentiation of orbital lymphoma from orbital inflammatory syndrome. Ophthal Plast Reconstr Surg 1997;13(2):129–134.
18. Sepahdari AR, Aakalu VK, Setabutr P, Shiehmorteza M, Naheedy JH, Mafee MF. Indeterminate orbital masses: restricted diffusion at MR imaging with echo-planar diffusion-weighted imaging predicts malignancy. Radiology 2010;256(2):554–564.
19. Shields CL, Shields JA. Lacrimal gland tumors. Int Ophthalmol Clin 1993;33(3):181–188.
20. Jung WS, Ahn KJ, Park MR, et al. The radiological spectrum of orbital pathologies that involve the lacrimal gland and the lacrimal fossa. Korean J Radiol 2007;8(4):336–342.
21. Mafee MF, Edward DP, Koeller KK, Dorodi S. Lacrimal gland tumors and simulating lesions: clinicopathologic and MR imaging features. Radiol Clin North Am 1999;37(1):219–239.
22. Bernardini FP, Devoto MH, Croxatto JO. Epithelial tumors of the lacrimal gland: an update. Curr Opin Ophthalmol 2008;19(5):409–413.
23. Rasmussen P, Ralfkiaer E, Prause JU, Sjö LD, Siersma VD, Heegaard S. Malignant lymphoma of the lacrimal gland: a nation-based study. Arch Ophthalmol 2011;129(10):1275–1280.

24. Lloyd GA. Lacrimal gland tumours: the role of CT and conventional radiology. Br J Radiol 1981;54 (648):1034–1038.
25. Politi LS, Forghani R, Godi C, et al. Ocular adnexal lymphoma: diffusion-weighted MR imaging for differential diagnosis and therapeutic monitoring. Radiology 2010;256(2):565–574.
26. Boukes RJ, de Vries-Knoppert WA. Lacrimal gland enlargement as one of the ocular manifestations of Wegener's granulomatosis. Doc Ophthalmol 1985; 59(1):21–26.
27. Raskin EM, McCormick SA, Maher EA, Della Rocca RC. Granulomatous idiopathic orbital inflammation. Ophthal Plast Reconstr Surg 1995;11 (2):131–135.
28. Avery RA, Fisher MJ, Liu GT. Optic pathway gliomas. J Neuroophthalmol 2011;31(3):269–278.
29. Kornreich L, Blaser S, Schwarz M, et al. Optic pathway glioma: correlation of imaging findings with the presence of neurofibromatosis. AJNR Am J Neuroradiol 2001;22(10):1963–1969.
30. Mafee MF, Goodwin J, Dorodi S. Optic nerve sheath meningiomas: role of MR imaging. Radiol Clin North Am 1999;37(1):37–58.
31. Kanamalla US. The optic nerve tram-track sign. Radiology 2003;227(3):718–719.
32. Miller NR. Primary tumours of the optic nerve and its sheath. Eye (Lond) 2004;18(11):1026–1037.
33. Garg R, Dhawan A, Gupta N, D'souza P. A rare case of benign isolated schwannoma in the inferior orbit. Indian J Ophthalmol 2008;56(6):514–515.
34. Xian J, Zhang Z, Wang Z, et al. Evaluation of MR imaging findings differentiating cavernous haemangiomas from schwannomas in the orbit. Eur Radiol 2010;20(9):2221–2228.
35. Messmer EP, Camara J, Boniuk M, Font RL. Amputation neuroma of the orbit: report of two cases and review of the literature. Ophthalmology 1984; 91(11):1420–1423.
36. De Potter P, Shields CL, Shields JA, Rao VM, Eagle RC Jr, Trachtenberg WM. The CT and MRI features of an unusual case of isolated orbital neurofibroma. Ophthal Plast Reconstr Surg 1992; 8(3):221–227.
37. Graeb DA, Rootman J, Robertson WD, Lapointe JS, Nugent RA, Hay EJ. Orbital lymphangiomas: clinical, radiologic, and pathologic characteristics. Radiology 1990;175(2):417–421.
38. Carroll GS, Haik BG, Fleming JC, Weiss RA, Mafee MF. Peripheral nerve tumors of the orbit. Radiol Clin North Am 1999;37(1):195–202.
39. Theos A, Korf BR; American College of Physicians; American Physiological Society. Pathophysiology of neurofibromatosis type 1. Ann Intern Med 2006;144(11):842–849.
40. Aydin MD, Yildirim U, Gundogdu C, Dursun O, Uysal HH, Ozdikici M. Malignant peripheral nerve sheath tumor of the orbit: case report and literature review. Skull Base 2004;14(2):109–113; discussion 113–114.
41. Spagnolo F, Caltabiano G, Queirolo P. Uveal melanoma. Cancer Treat Rev 2012;38(5):549–553.
42. Grin JM, Grant-Kels JM, Grin CM, Berke A, Kels BD. Ocular melanomas and melanocytic lesions of the eye. J Am Acad Dermatol 1998;38(5 Pt 1): 716–730.
43. Shields CL, Shields JA, Materin M, Gershenbaum E, Singh AD, Smith A. Iris melanoma: risk factors for metastasis in 169 consecutive patients. Ophthalmology 2001;108(1):172–178.
44. The Collaborative Ocular Melanoma Study (COMS) randomized trial of pre-enucleation radiation of large choroidal melanoma I: characteristics of patients enrolled and not enrolled. COMS report no. 9. Am J Ophthalmol 1998;125(6):767–778.
45. Mafee MF. Uveal melanoma, choroidal hemangioma, and simulating lesions: role of MR imaging. Radiol Clin North Am 1998;36(6):1083–1099.
46. Lemke AJ, Hosten N, Bornfeld N, et al. Uveal melanoma: correlation of histopathologic and radiologic findings by using thin-section MR imaging with a surface coil. Radiology 1999;210(3):775–783.
47. De Potter P, Shields JA, Shields CL, Yannuzzi LA, Fisher YE, Rao VM. Unusual MRI findings in metastatic carcinoma to the choroid and optic nerve: a case report. Int Ophthalmol 1992;16(1):39–44.
48. Freedman MI, Folk JC. Metastatic tumors to the eye and orbit: patient survival and clinical characteristics. Arch Ophthalmol 1987;105(9):1215–1219.
49. Shields JA, Shields CL, Brotman HK, Carvalho C, Perez N, Eagle RC Jr. Cancer metastatic to the orbit: the 2000 Robert M. Curts Lecture. Ophthal Plast Reconstr Surg 2001;17(5):346–354.
50. Shields CL, Shields JA, Gross NE, Schwartz GP, Lally SE. Survey of 520 eyes with uveal metastases. Ophthalmology 1997;104(8):1265–1276.
51. Ahmad SM, Esmaeli B. Metastatic tumors of the orbit and ocular adnexa. Curr Opin Ophthalmol 2007; 18(5):405–413.
52. Goldberg RA, Rootman J, Cline RA. Tumors metastatic to the orbit: a changing picture. Surv Ophthalmol 1990;35(1):1–24.
53. Meltzer DE, Chang AH, Shatzkes DR. Case 152: orbital metastatic disease from breast carcinoma. Radiology 2009;253(3):893–896.
54. Koyama T, Ueda H, Togashi K, Umeoka S, Kataoka M, Nagai S. Radiologic manifestations of sarcoidosis in various organs. RadioGraphics 2004;24 (1):87–104.

RadioGraphics

Orbital Neoplasms in Adults: Clinical, Radiologic, and Pathologic Review[1]

Tina D. Tailor, MD • Divakar Gupta, MD • Roberta W. Dalley, MD C. • Dirk Keene, MD, PhD
Yoshimi Anzai, MD, MPH

RadioGraphics 2010; 30:461–482 • **Published online** 10.1148/rg.302095115 • **Content Codes:** HN MR NR OI

Page 1742
Although not true neoplasms, cavernous malformations are the most common benign orbital mass in adults.

Page 1745
One feature of these tumors is their tendency to mold to orbital structures, such as the globe, optic nerve, and orbital wall; tumor shaped around the latter may result in bone remodeling.

Page 1749
However, because the substance of the nerve is spared, a "tram-track" configuration is often observed at axial contrast-enhanced CT or MR imaging, since enhancing tumor lies on either side of the nerve.

Page 1754
MR imaging is superior to CT in the evaluation of choroidal melanomas, as melanin has intrinsic T1 and T2 shortening effects, thereby manifesting with increased T1 signal intensity and decreased T2 signal intensity.

Page 1754
Metastatic breast cancer is the most common type to metastasize to the orbit, accounting for 48%–53% of orbital metastases, followed by metastatic prostate carcinoma, melanoma, and lung cancer.